Supporting Information for

Understanding Contact Electrification *via* Direct Covalent Bond Cleavage of Polymer Chains for Ultrahigh Electrostatic Charge Density

Haiyan Fu, Jianliang Gong*, Junhao Cao, Zehua Zhang, Zuchang Long, Bao Yang, Jianzhuang Chen, Yiwang Chen*, Xiaoming Tao

*To whom correspondence should be addressed.

E-mail: jlgong@jxnu.edu.cn; ywchen@ncu.edu.cn

Experimental Methods

Materials: Viscoelastic polymer adhesives (VPAs) were derived from the adhesive side of commercially available transparent adhesive tape or double-sided adhesive tape. The main components of these adhesive taps are polyacrylates. The dielectric material of polypropylene (PP), polyethylene (PE), polyethylene terephthalate (PET) and polytetrafluoroethylene (PTFE) were consumer-grade materials easily available in the market. Copper/nickel coated polyester fabric (CNF) laminated with a layer of polyacrylates adhesives was bought from 3M Corp. The conductive material was also a common material on the market. The radical scavengers of 2,2-Diphenyl-1-picrylhydrazyl (DPPH) was acquired from Merck company. The $HAuCl_4$, $AgNO_3$ and $Cu(acac)_2$ metal compound purchased from Aladdin Corporation. All materials were used as received without further purification.

Preparation of VPA or radical scavenger-doped VPA films deposited by metal nanoparticles (NPs)

The contacted VPA films were immersed in an aqueous solution of $HAuCl_4$, $Cu(acac)_2$, and $AgNO_3$ (each 4 mg/mL in H_2O) for 48 h, metal NPs were deposited on the VPA films surface to form VPA-Au, VPA-Cu and VPA-Ag films. The samples of VPA-DPPH-Au, VPA-DPPH-Cu and VPA-DPPH-Ag were obtained by first immersing the contacted films into a 4 mg/L DPPH solution for 2 h and then kept in 4 mg/mL $HAuCl_4$, $Cu(acac)_2$, and $AgNO_3$ solution for 48 h.

Assembly of adhesive surface-enabled TENGs (AS-TENGs)

A typical AS-TENG was assembled based on a vertical contact-separation mode by using the VPA surface and different material as CE pairs. Two pieces of CNFs were laminated on the noncontact surfaces of the pairing material and CNF as electrodes, respectively.

CE performance evaluation of VPA films contacted by different pairing materials

The CE performance of VPA (PE, PP or PET) films was quantitatively evaluated by fixing a kind of dielectric material PTFE or conductive material CNF as pairing material. The pairing material was driven by an external force of ~600 N to repetitively impact the surface of VPA film. The contacted VPA films were used to react with DPPH solution for quantifying the generated mechanoradicals, while the electrostatic charges of VPA films caused by CE were quantitatively evaluated by the combination of electrostatic induction effect to measure their transferred charges. Unless otherwise specified, the test environment condition was consistent, where the temperature was 298 K and the relative humidity was about 50%.

Quantitative evaluation of mechanoradical density (ρ(R)) by DPPH consumption reaction

To further quantitatively investigated the density of mechanoradical (ρ(R)) of the VPA films generated on CE by applying DPPH consumption reaction. Assuming that all types of mechanoradicals generated by bond scission have the same reactivity in the DPPH solution, ρ(R) could be considered equal to the consumption of DPPH

concentration. Thus, the ρ(R) was written as

$$\rho(R)=(C_{DPPH}\times V_{DPPH}\times R_{DPPH}\times N_A)/A_{VPA}$$

where R_{DPPH} stand for the ratio of DPPH degradation (%, the difference between the absorption intensity of the DPPH solution soaked by VPA and the original solution), C_{DPPH} was the concentration of pristine DPPH (0.01mol/L), V_{DPPH} was the volume of DPPH used, N_A was Avergadro's constant (6.02×10^{23}/mol) and A_{VPA} was the area of the VPA (cm^2).

Energy calculations method for homolytic and heterlytic breakage of C-C bonds in polyacrylates

All calculations were carried out with the Gaussian 16 software. The Becke Lee-Yang-Parr (B3LYP) functional was adopted for all calculations. For geometry optimization and frequency calculations, the 6-311G(d) basis set was used, and the optimal geometry for each compound was determined. The singlet point energy calculations were performed with a larger basis set the 6-311+G(dp) basis set. The DFT-D3 dispersion correction with BJ-damping was applied to correct the weak interaction to improve the calculation accuracy. Then, the Bond Energy was calculated by the following formula BDE=(EpartA+EpartB)-Emol.[1]

Energy calculations method for charge distribution on the main chain C-C bond of polyacrylates in the presence/absence of water

The charge distribution on the main chain C-C bond in the presence/absence of water

in polyacrylates was compared by using both “Hirshfeld Atomic Populations” and “Voronoi Atomic Populations” calculations. [2]

Characterization

All scanning electron microscopy images were obtained on a field emission scanning electron microscope (FESEM, CLARA) equipped with an energy-dispersive X-ray spectroscopy (EDS) detector. The UV-Vis absorption spectra of radical scavengers reacted with different VPA films were monitored a UV-Vis spectrometer (Lamda 1050+, PerkinElmer). X-ray photoelectron spectroscopy (XPS) spectra were recorded on a Kratos Model XSAM800 XPS spectrometer. The contact electrification process between VPA and PTFE was recorded with a high-speed camera (Revealer). The surface morphology of the material contacted by VPA was characterized by atomic force microscope (AFM, Bruker Dimension Icon). The Fourier Infrared Spectroscopy (FT-IR, Thermo) was used to detect groups in polymer materials. The adhesion force between VPA/pair materials was tested utilizing a universal tensile machine (Shimadzu, AGS-X). The mechanical force applied on testing the stability and charging capacity was generated by a ~60 kg adult male or customized fatigue testing machine with adjustable loading weight. Electrostatic charges were measured via using a Keithley 6514 electrometer under coulombs measurement mode.

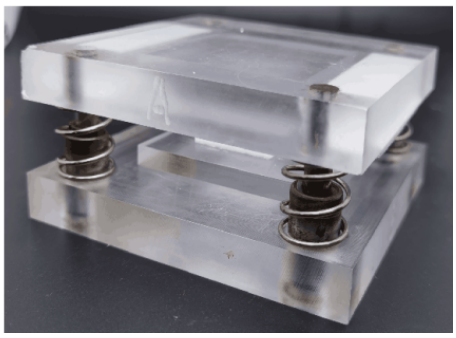

Figure S1. Digital photograph of a custom-made device with a double-layer structure for CE between two different materials to generate electrostatic charges and mechanoradicals. It is consisted of an insulating plate fixed with a VPA/electrode layer and another insulating plate fixed with an identical-size pairing material/electrode layer. Four springs are installed at their corners to leave a distance between the surface of the VPAs and PTFE film. They allow the contact of VPAs with PTFE by external force and enable their separation after the release of external force.

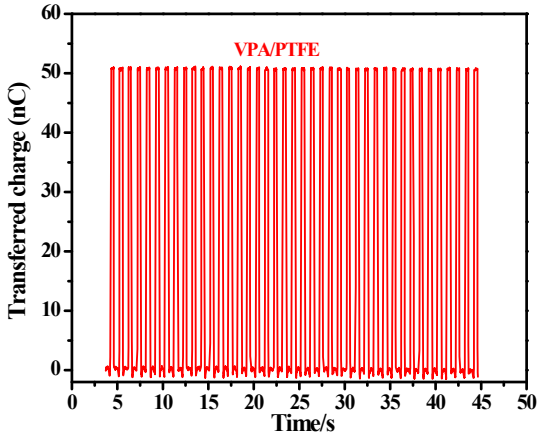

Figure S2. Typical electrostatic charge curve generated by a cyclic impact force using PTFE film and polyacrylate adhesive layer as CE pairs.

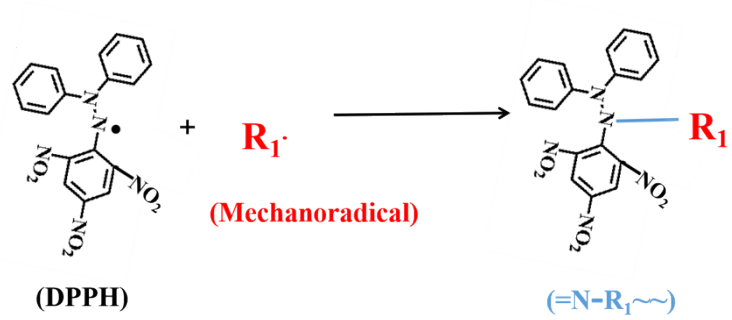

Figure S3. Schematic of chain termination reaction between mechanoradicals generated by CE and the radical scavenger DPPH.

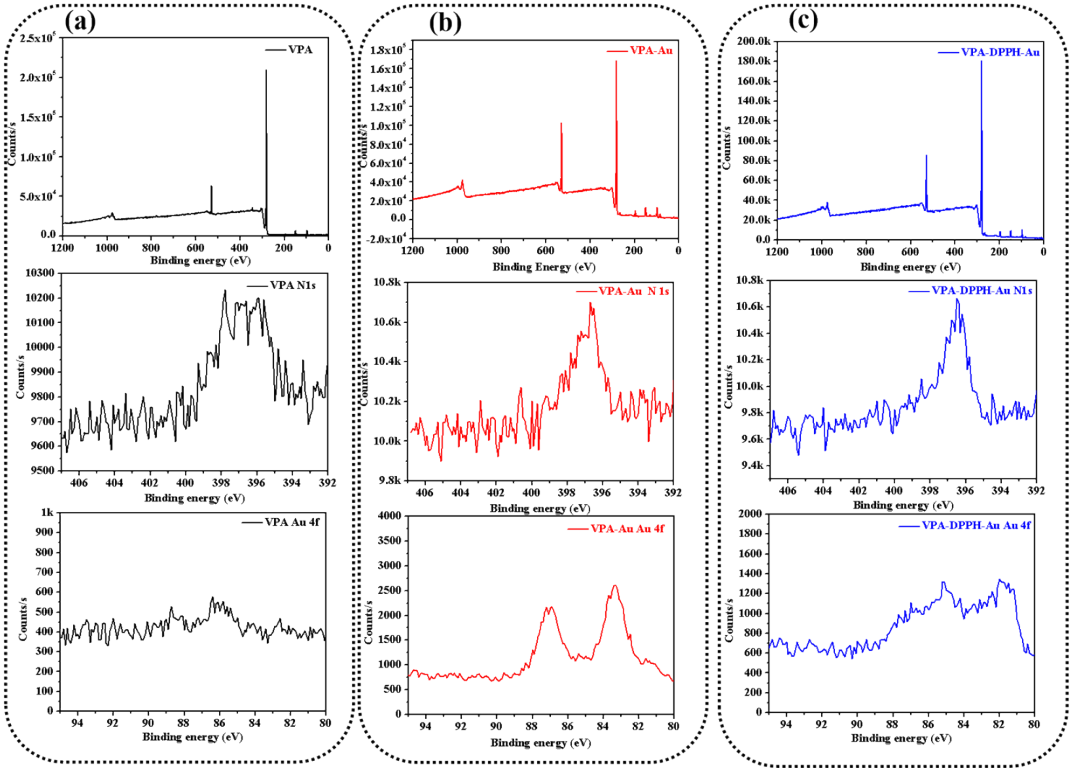

Figure S4. XPS spectra of (a) pure VPA film, (b) the VPA film after immersion in the $HAuCl_4$ (aq) for 48 h, and (c) a VPA film first immersed into a 4 mg/L DPPH solution for 2 h and then kept in $HAuCl_4$ (aq) for 48 h.

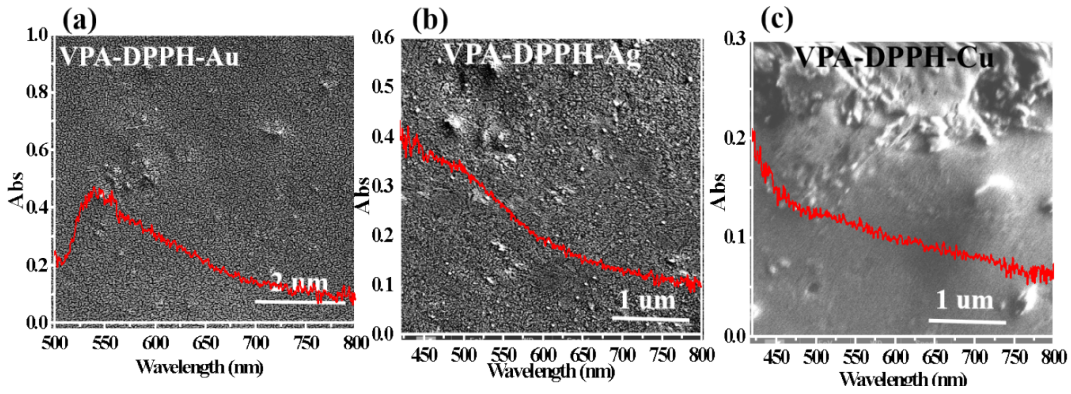

Figure S5. SEM images of VPA films first immersed into a DPPH solution for 2 h and then kept in aqueous solution of (a) $HAuCl_4$, (b) $AgNO_3$, and (c) $Cu(acac)_2$ for 48 h. The red lines were the UV/vis spectrum of the related samples of VPA-DPPH-Au, VPA-DPPH-Ag and VPA-DPPH-Cu.

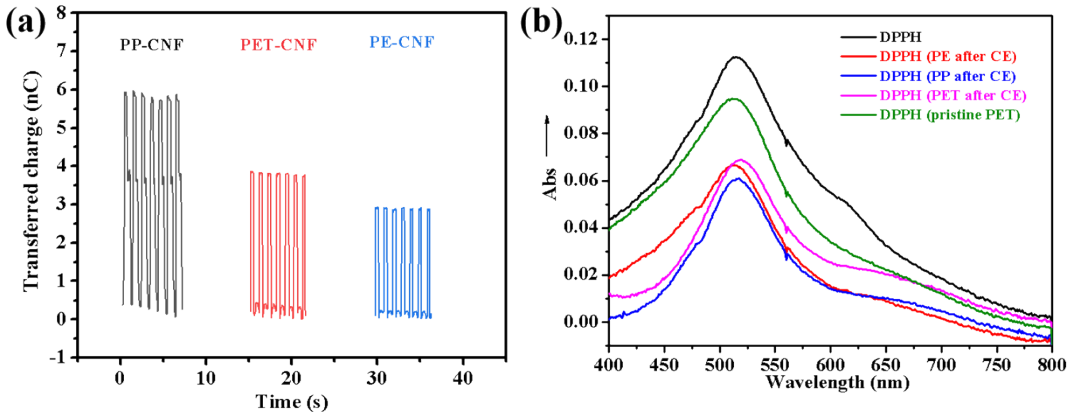

Figure S6. Non-adhesive polymers polyethylene (PE), polypropylene (PP) and polyester (PET) generated both electric charge and mechanoradicals during CE process. (a) The typical electrostatic charge curves of non-adhesive polymer films after CE with CNF, (b) typical UV/Vis spectrum of DPPH solutions immersed with PET, PP and PE after CE with CNF, and pristine PET, respectively.

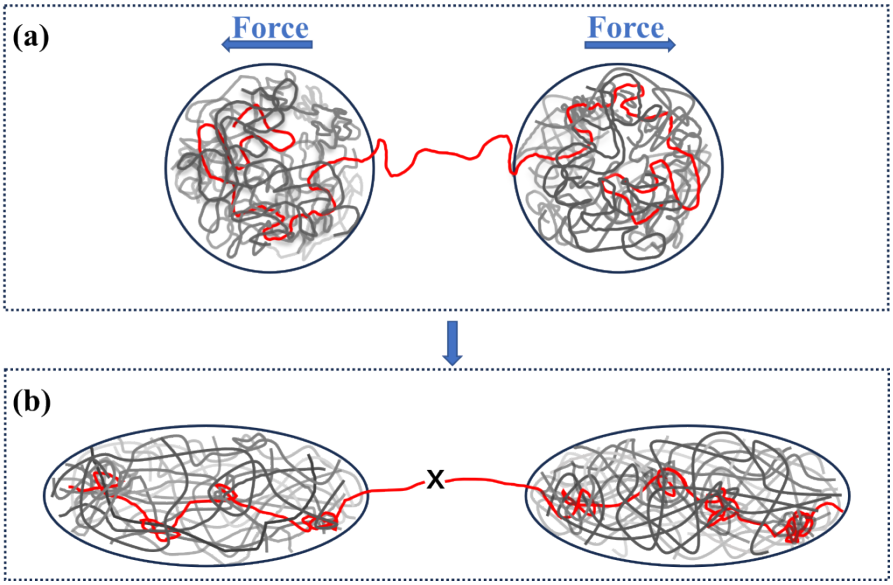

Figure S7. Polymer chain "wool cluster" breakage model. During the contact/separation of two polymer materials, when one of the polymer chains was entangled and bounded by the other polymer chains at both ends, it would inevitably cause fracture under the continuous action of external force.

Table S1. Comparison of dissociation energies of C-C bond of main chain in polyacrylates (ΔE_{diss}(C-C)) obtained with theoretical methods to the experimental data.

ΔE_{diss}(C−C) / Method	Radicaloid Bond Breaking (kJ mol^{-1})	Ionic Bond Breaking (kJ mol^{-1})
B3LYP	341.13	1166.80
Experiment	359.19 ± 11.85	~

Table S2. Comparison of charge distribution on main-chain C-C bonds ($Q_{distri}(C-C)$) in polyacrylates in the presence/absence of water.

$Q_{distri}(C-C)$ Method	Without H_2O (eV)	With H_2O (eV)
Hirshfeld Atomic Analysis	0.15824	0.16587
Voronoi Atomic Analysis	0.17391	0.18066

Table S3. The effect of humidity on charge density and mechanoradicals generated via CE.

RH (%)	Charge density ($\rho(Q)$, nC/cm^2)	Ratio of DPPH Degradation ($R_{DPPH}\%$)	Concentration of radical ($\rho(R)$, $10^{15}/cm^2$)
19.7	26.64±1.36	80.60±1.16	2.69±0.009
22.9	35.57±1.20	79.69±1.30	2.66±0.011
33.5	65.23±2.05	78.24±1.05	2.61±0.008
44.0	52.65±1.74	77.11±1.54	2.58±0.013
52.8	47.28±1.63	76.94±1.66	2.57±0.014
68.0	15.10±1.23	75.64±1.33	2.54±0.011
76.5	12.20±1.32	73.22±1.42	2.45±0.012

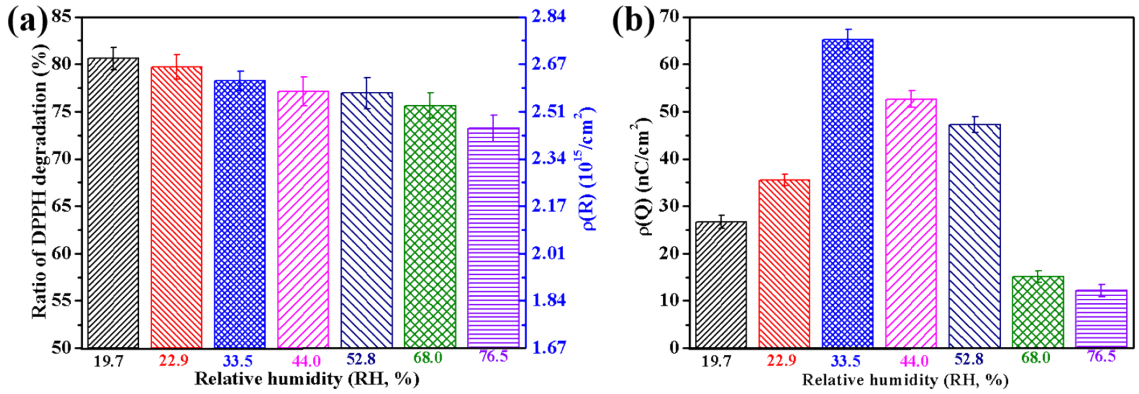

Figure S8. (a) Degradation performance comparison of DPPH with VPA mechanoradicals and (b) comparison of ρ(Q) of VPAs under different RH.

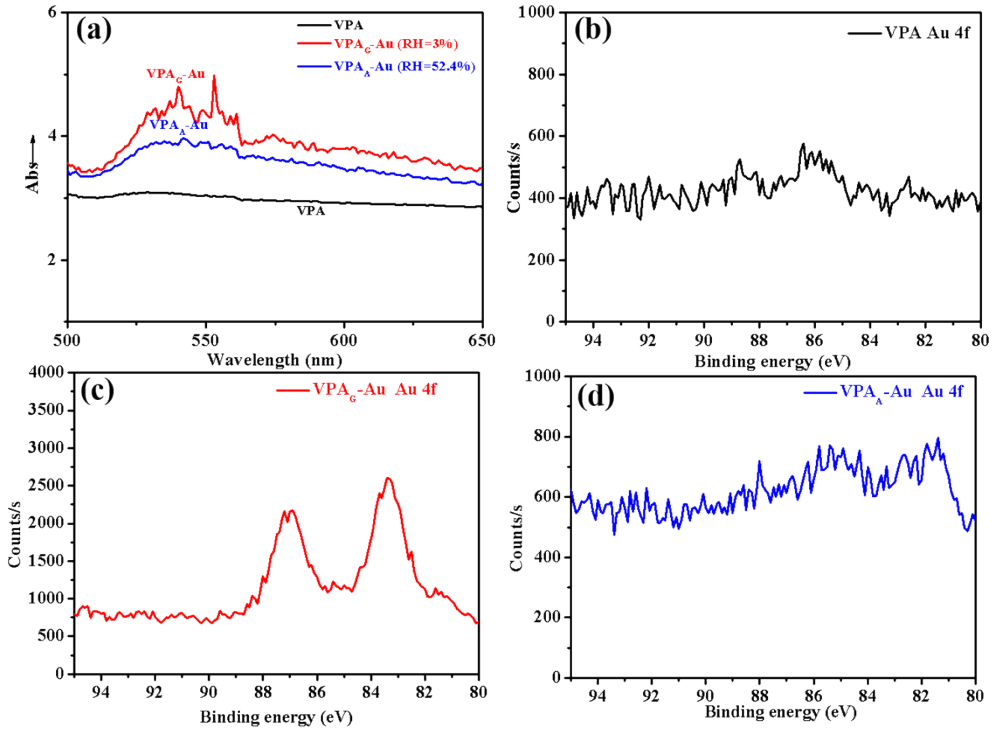

Figure S9. Comparison of the reduction capacity of Au^{2+} by mechanoradicals generated on the surface of VPA at different humidity levels. (a) The UV/vis of pristine VPA film, VPA_G-Au and VPA_A-Au; the XPS spectrum of (b) VPA, (c) VPA_G-Au and (d) VPA_A-Au featuring the Au 4f peak characteristic of Au NPs.

Table S4. Comparison of elemental content of VPA film, VPA_G-Au and VPA_A-Au samples.

Sample	C	O	Si	N	Au
VPA	90.04	5.78	3.65	0.54	0
VPA_A-Au	80.32	10.58	6.38	0.45	0.05
VPA_G-Au	77.54	12.48	6.62	0.43	0.08

Table S5. Comparison of the adhesion forces between different VPA with PTFE and the effect on the ρ(Q) and ρ(R) generated between them via CE.

Sample	**Adhension strength (MPa)**	**ρ(Q) (nC/cm^2)**	**Ratio of DPPH Degradation (R_{DPPH}%)**	**ρ(R) ($10^{15}/cm^2$)**
VPA_M	3.24±0.50	90.31±1.33	81.39±1.22	2.72±0.041
VPA_L	2.43±0.33	74.58±2.05	79.59±1.45	2.65±0.048
VPA	2.31±0.05	65.25±1.74	77.62±1.94	2.59±0.065
VPA_S	1.87±0.31	54.31±1.63	59.15±1.42	1.98±0.047

Table S6. The ρ(Q) of polyethylene (PE) generated via CE in the open environment in the reported literature.

PE / Number	Charge density (nC/cm^2)	Ref.

1	0.5-50	[3]
2	5	[4]
3	9.5	[5]
4	1.2	[5]
5	5.0	[5]
6	1.26	[6]
7	7.12	[7]

Table S7. The ρ(Q) of PTFE generated via CE in the open environment in the reported literature.

PTFE / Number	Charge density (nC/cm^2)	Ref.
1	7	[3]
2	0.05	[8]
3	12	[9]
4	2.75	[6]
5	8.5	[10]
6	11.3	[7]
7	10	[11]

Table S8. The ρ(Q) of polyethylene terephthalate (PET) generated via CE in the open environment in the reported literature.

PET Number	Charge density (nC/cm^2)	Ref.
1	7.5	[12]
2	6.25	[12]
3	0.1	[6]
4	4.9	[13]
5	8.94	[8]
6	20	[11]
7	7.65	[14]

Table S9. The ρ(Q) of polyamide (PA) generated via CE in the open environment in the reported literature.

PA Number	Charge density (nC/cm^2)	Ref.
1	0.283	[6]
2	4.9	[13]
3	2.5	[7]
4	10	[15]
5	6	[16]

Table S10. The ρ(Q) of fluorinated ethylene propylene (FEP) generated via CE in the open environment in the reported literature.

FEP Number	Charge density (nC/cm^2)	Ref.
1	4	[17]
2	5	[18]
3	24	[18]
4	22	[5]
5	6.8	[19]
6	14	[19]
7	12.09	[20]
8	11	[21]
9	4.9	[13]
10	3.2	[22]
11	8.125	[23]
12	16.56	[15]
13	35.2	[24]

Table S11. The ρ(Q) of polydimethylsiloxane (PDMS) generated via CE in the open environment in the reported literature.

PDMS / Number	Charge density (nC/cm^2)	Ref.
1	0.16	[25]
2	2	[26]
3	0.018123	[27]
4	19	[28]
5	36	[29]
6	35	[30]
7	0.020695	[31]
8	0.006675	[31]
9	20.695	[31]
10	5.45	[32]
11	5.23	[33]

Table S12. The ρ(Q) of VPA generated via CE in the open environment in the reported literature.

VPA / Number	Charge density (nC/cm^2)	Ref.
1	10	[34]

2	4.68	[35]
3	3.69	[36]
4	14.65	[37]
5	90.31	This work

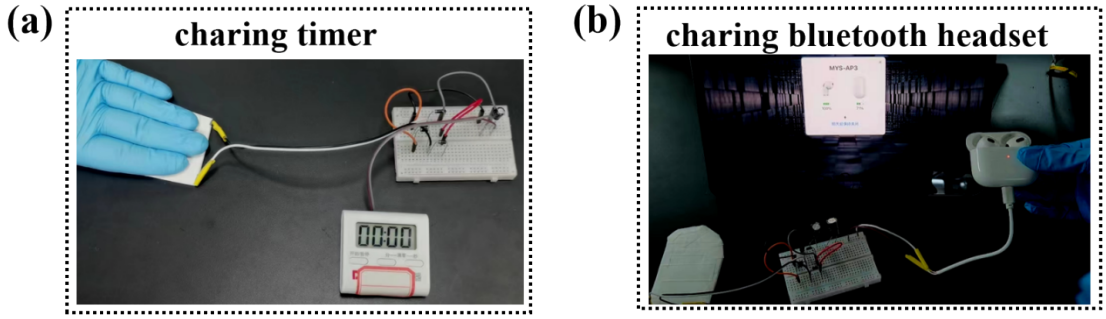

Figure S10. The use of AS-TENGs for driving (a) timers and (b) Bluetooth headsets

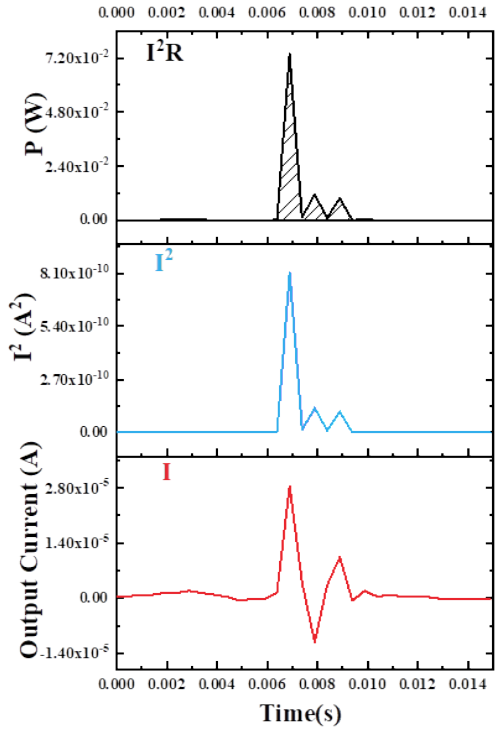

Figure S11. The typical output energy curve generated by AS-TENG (1 cm^2) with a single step. Based on this curve, the energy produced by AS-TENG with a single cycle can be calculated:

$$E_{cycle} = \int_0^t I^2 R dt = 4.92 \times 10^{-5} J/cm^2$$

Where E_{cycle}, I, and R represent the electric energy generated of AS-TENG with effective electricity generation area of 1 cm^2 by a single cycle, the instantaneous current at t, and external resistance (R=8 MΩ), respectively.

If A=10 cm^2, assuming that a person walks 5,000 steps (N_{step}) per day, the energy produced was:

$$E_{5000} = E_{cycle} \times A \times N_{step} = 4.92 \times 10^{-5} \times 10 \times 5000 = 2.46 J$$

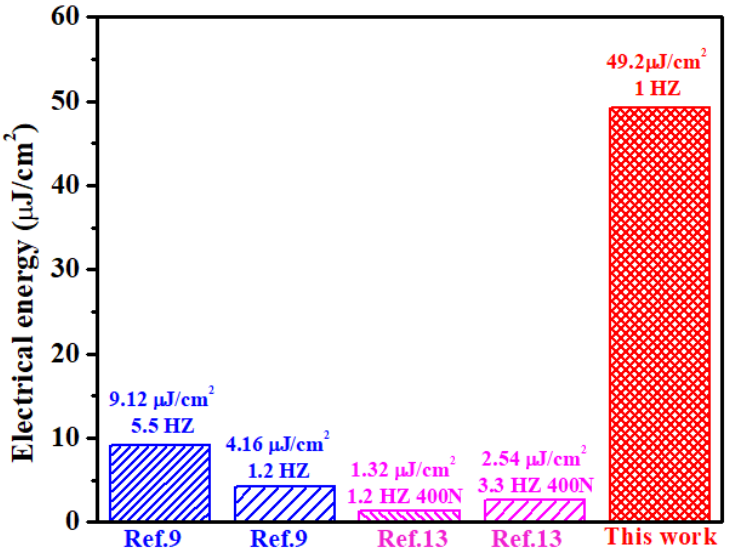

Figure S12. Comparison of the energy generated by one cycle in the CE process.

References

[1] a) A. D. Becke, *The Journal of Chemical Physics* **1993**, *98*, 5648-5652; b) S. Grimme, S. Ehrlich, L. Goerigk, *Journal of computational chemistry* **2011**, *32*, 1456-1465; c) R. Krishnan, J. S. Binkley, R. Seeger, J. A. Pople, *The Journal of chemical physics* **1980**, *72*, 650-654.

[2] L. Bengtsson, *Physical Review B* **1999**, *59*, 12301.

[3] D. Donald, *Journal of the Electrochemical Society* **1968**, *115*, 270.

[4] H. Haenen, *Journal of Electrostatics* **1976**, *2*, 151-173.

[5] Y. Zi, S. Niu, J. Wang, Z. Wen, W. Tang, Z. L. Wang, *Nature communications* **2015**, *6*, 8376.
[6] S. Liu, W. Zheng, B. Yang, X. Tao, *Nano Energy* **2018**, *53*, 383-390.
[7] H. Zou, Y. Zhang, L. Guo, P. Wang, X. He, G. Dai, H. Zheng, C. Chen, A. C. Wang, C. Xu, *Nature communications* **2019**, *10*, 1427.
[8] J. Zhong, Q. Zhong, F. Fan, Y. Zhang, S. Wang, B. Hu, Z. L. Wang, J. Zhou, *Nano Energy* **2013**, *2*, 491-497.
[9] J. Wang, C. Wu, Y. Dai, Z. Zhao, A. Wang, T. Zhang, Z. L. Wang, *Nature communications* **2017**, *8*, 88.
[10] B. D. Chen, W. Tang, C. Zhang, L. Xu, L. P. Zhu, L. J. Yang, C. He, J. Chen, L. Liu, T. Zhou, *Nano Research* **2018**, *11*, 3096-3105.
[11] S. Li, Y. Fan, H. Chen, J. Nie, Y. Liang, X. Tao, J. Zhang, X. Chen, E. Fu, Z. L. Wang, *Energy Environmental Science* **2020**, *13*, 896-907.
[12] S.-H. Shin, Y. E. Bae, H. K. Moon, J. Kim, S.-H. Choi, Y. Kim, H. J. Yoon, M. H. Lee, J. Nah, *ACS nano* **2017**, *11*, 6131-6138.
[13] L. Cheng, Q. Xu, Y. Zheng, X. Jia, Y. Qin, *Nature Communications* **2018**, *9*, 3773.
[14] P. Chen, Y. Luo, R. Cheng, S. Shu, J. An, A. Berbille, T. Jiang, Z. L. Wang, *Advanced Energy Materials* **2022**, *12*, 2201813.
[15] J. Qian, J. He, S. Qian, J. Zhang, X. Niu, X. Fan, C. Wang, X. Hou, J. Mu, W. Geng, *Advanced Functional Materials* **2020**, *30*, 1907414.
[16] C. Xing, Y. Tian, Z. Yu, Z. Li, B. Meng, Z. Peng, *ACS Applied Materials interfaces Interfaces* **2022**, *14*, 36741-36752.
[17] G. Zhu, Y. Su, P. Bai, J. Chen, Q. Jing, W. Yang, Z. L. Wang, *ACS Nano* **2014**, *8*, 6031-6037.
[18] S. Wang, Y. Xie, S. Niu, L. Lin, C. Liu, Y. S. Zhou, Z. L. Wang, *Advanced Materials* **2014**, *26*, 6720-6728.
[19] S. Wang, Y. Zi, Y. S. Zhou, S. Li, F. Fan, L. Lin, Z. L. Wang, *Journal of Materials Chemistry A* **2016**, *4*, 3728-3734.
[20] S. Han, F. Jiao, Z. U. Khan, J. Edberg, S. Fabiano, X. Crispin, *Advanced Functional Materials* **2017**, *27*, 1703549.
[21] N. Wu, H. Jiang, W. Li, S. Lin, J. Zhong, F. Yuan, L. Huang, B. Hu, J. Zhou, *Journal of Materials Chemistry A* **2017**, *5*, 12787-12792.
[22] Z. Saadatnia, E. Esmailzadeh, H. E. Naguib, *Advanced Engineering Materials* **2019**, *21*, 1700957.
[23] S. Nie, C. Cai, X. Lin, C. Zhang, Y. Lu, J. Mo, S. Wang, *ACS Sustainable Chemistry Engineering* **2020**, *8*, 18678-18685.
[24] Z. Liu, Y. Huang, Y. Shi, X. Tao, H. He, F. Chen, Z.-X. Huang, Z. L. Wang, X. Chen, J.-P. Qu, *Nature Communications* **2022**, *13*, 4083.
[25] H. Baytekin, A. Patashinski, M. Branicki, B. Baytekin, S. Soh, B. A. Grzybowski, *Science* **2011**, *333*, 308-312.
[26] H. T. Baytekin, B. Baytekin, T. M. Hermans, B. Kowalczyk, B. A. Grzybowski, *Science* **2013**, *341*, 1368-1371.
[27] X. He, H. Guo, X. Yue, J. Gao, Y. Xi, C. Hu, *Nanoscale* **2015**, *7*, 1896-1903.

[28] J. Chen, H. Guo, X. He, G. Liu, Y. Xi, H. Shi, C. Hu, *ACS applied materials interfaces* **2016**, *8*, 736-744.
[29] L. Shi, S. Dong, P. Ding, J. Chen, S. Liu, S. Huang, H. Xu, U. Farooq, S. Zhang, S. Li, *Nano Energy* **2019**, *55*, 548-557.
[30] K. Shi, H. Zou, B. Sun, P. Jiang, J. He, X. Huang, *Advanced Functional Materials* **2020**, *30*, 1904536.
[31] G. Z. Li, G. G. Wang, D. M. Ye, X. W. Zhang, Z. Q. Lin, H. L. Zhou, F. Li, B. L. Wang, J. C. Han, *Advanced Electronic Materials* **2019**, *5*, 1800846.
[32] H. G. Menge, J. O. Kim, Y. T. Park, *Materials today* **2020**, *13*, 4156.
[33] P. Zhang, W. Zhang, L. Deng, H. Zhang, *Nano Energy* **2021**, *87*, 106176.
[34] H. T. Baytekin, B. Baytekin, S. Huda, Z. Yavuz, B. A. Grzybowski, *Journal of the American Chemical Society* **2015**, *137*, 1726-1729.
[35] J. Gong, B. Xu, Y. Yang, M. Wu, B. Yang, *Advanced Materials* **2020**, *32*, 1907948.
[36] H. Fu, J. Gong, H. Zhong, B. Yang, Z. Long, J. Zeng, Z. Cheng, J. He, B. Xu, Y. Chen, *Journal of Materials Chemistry A* **2022**, *10*, 9643-9654.
[37] K. Shi, B. Chai, H. Zou, Z. Wen, M. He, J. Chen, P. Jiang, X. Huang, *Advanced Functional Materials* **2023**, *33*, 2307678.